AIAA JOURNAL
Vol. 30, No. 11, November 1992

Generalized Multipoint Inverse Airfoil Design

Michael S. Selig* and Mark D. Maughmer†
Pennsylvania State University, University Park, Pennsylvania 16802

In a rather general sense, inverse airfoil design can be taken to mean the problem of specifying a desired set of airfoil characteristics, such as the airfoil maximum thickness ratio, pitching moment, part of the velocity distribution, or boundary-layer development. From this information, the corresponding airfoil shape is determined. This paper presents a method that approaches the design problem from this perspective. In particular, the airfoil is divided into segments along which, together with the design conditions, either the velocity distribution or boundary-layer development may be prescribed. In addition to these local desired distributions, single parameters like the airfoil thickness can be specified. Determination of the airfoil shape is accomplished by coupling an incompressible potential-flow inverse airfoil design method with a direct integral boundary-layer analysis method. The resulting system of nonlinear equations is solved by a multidimensional Newton iteration technique. An example airfoil design, not intended for practical application, is presented to illustrate some of the capabilities of the method. As this example illustrates, the design methodology presented provides a means of dealing simultaneously with the myriad requirements and constraints that can be specified in the design of an airfoil.

Nomenclature

a_m, b_m = Fourier series coefficients
c = airfoil chord
c_m = pitching-moment coefficient for a given angle of attack
c_{m_0} = pitching-moment coefficient at zero lift
$F(z)$ = complex potential function
I = total number of airfoil segments
K = main recovery parameter
K_H = closure recovery parameter
K_S = trailing-edge thickness parameter
$P(\phi)$ = harmonic function on circle
p = value of a desired generic parameter
$Q(\phi)$ = conjugate harmonic function on circle
s = arc length about airfoil
s_i = arc length for segment i
$\bar{s}_i$ = relative arc length for segment i
t/c = maximum thickness ratio of airfoil
V = freestream velocity ($V = 1$)
v = airfoil velocity distribution normalized by freestream velocity
v_i = velocity level for segment i
$v^*(\phi)$ = multipoint design velocity distribution
$\bar{v}_i(\bar{\phi}_i)$ = relative design velocity distribution as a function of $\bar{\phi}_i$ for segment i
$\bar{v}_i(\bar{s}_i)$ = relative design velocity distribution as a function of $\bar{s}_i$ for segment i
$w(\phi)$ = total recovery function
$w_F(\phi)$ = trailing-edge recovery function
$w_S(\phi)$ = closure recovery function
$w_W(\phi)$ = main recovery function
z = physical-plane complex coordinate ($x + iy$)
α = angle of attack from zero-lift angle
α_{OL} = zero-lift angle of attack relative to airfoil chordline
$\alpha^*(\phi)$ = multipoint design angle-of-attack distribution
ϵ = trailing-edge included angle parameter
ζ = circle-plane complex coordinate ($\xi + i\eta$)
$\theta^*(\phi)$ = local direction of flow about airfoil
μ = main recovery parameter
$\pi^*(\phi)$ = step function
ϕ = arc limit in circle plane
ϕ_i = arc limit for segment i
$\phi_{i_{LE}}$ = leading-edge arc limit
ϕ_F = trailing-edge recovery arc limit
ϕ_S = closure recovery arc limit
ϕ_W = main recovery arc limit
$\bar{\phi}_i$ = relative arc limit for segment i

Boundary-Layer Variables

c_D = dissipation coefficient
c_f = skin-friction coefficient
H_{12}, H_{32} = shape factors, δ_1/δ_2 and δ_3/δ_2
n = linear stability amplification factor
R = airfoil chord Reynolds number, Vc/ν
R_{δ_2} = Reynolds number, $v\delta_2/\nu$
δ_1, δ_2, δ_3 = displacement, momentum, and energy thicknesses
ν = kinematic viscosity

Subscript

i = value for segment or at arc limit ϕ_i

Superscripts

$\bar{}$ = relative to beginning of segment
$^-$ = lower-surface quantity
^{i} = Newton node index

Introduction

TRADITIONALLY, inverse airfoil design is considered as the problem of finding the airfoil shape corresponding to a specified velocity distribution. To more directly control the airfoil characteristics, the contemporary view of inverse airfoil design follows principally along two lines of thought. First, emphasis is being placed on solving multipoint design problems either by inverse formulations[1,2] or numerical optimization.[3,4] Second, there is continued interest in prescribing quantities other than just the velocity distribution. For instance, it

Presented as Paper 91-3333 at the AIAA 9th Applied Aerodynamics Conference, Baltimore, MD, Sept. 23-25, 1991; received Oct. 17, 1991; revision received April 30, 1992; accepted for publication May 6, 1992.

*Research Assistant, Department of Aerospace Engineering, 233 Hammond Building; currently Assistant Professor, Department of Aeronautical and Astronautical Engineering, University of Illinois at Urbana-Champaign, Urbana, IL 61801. Member AIAA.

†Associate Professor, Department of Aerospace Engineering, 233 Hammond Building. Senior Member AIAA.

is often the case that the designer wishes to specify local flow physics such as the boundary-layer shape factor[5-10] or a Stratford turbulent pressure recovery.[11] In other cases, it may be desirable to control the geometry over a segment of the airfoil.[12] Besides specification of these desired local distributions, it is usually necessary to simultaneously achieve global parameters such as the thickness ratio and pitching moment. Thus, in broad terms, a modern airfoil design methodology should allow for multipoint design, as well as for the selection and specification of the independent design variables, be they the velocity distribution, boundary-layer development, or single design parameters.

This paper presents an approach to solving this general problem by coupling a boundary-layer analysis procedure with an inverse airfoil design method developed earlier.[2,13] Then, through a convenient parameterization of the desired design variables and appropriately selected dependent variables, the nonlinear system is solved via Newton iteration. The method is highly flexible. For instance, it is possible to specify the airfoil velocity distribution on the upper surface at one angle of attack and some boundary-layer development on the lower surface at a different angle of attack, while at the same time achieving a desired airfoil thickness ratio and pitching moment. Of course, these prescribed conditions are subject to the constraints that the airfoil shape must be closed and uncrossed and that the velocity distribution must be continuous.

Formulation of the Problem

Although a number of schemes have been devised to achieve desired velocity distribution,[1-4,11,12,14-21] there are only two common approaches for the achievement of a desired boundary-layer development. One approach[6,7,11] is to use an inverse boundary-layer method to determine the velocity distribution that yields the desired boundary-layer development, typically the shape-factor or skin-friction distribution. The resulting velocity distribution is then used as input to a potential-flow inverse airfoil method that provides the corresponding airfoil shape.

The disadvantage of the method is that only single-point design problems can be handled directly. Whether or not the resulting airfoil meets the multipoint design requirements is determined through postdesign analysis. If discrepancies do exist, part of the velocity distribution is modified judiciously until the desired goals are eventually achieved. Another difficulty arises when the boundary-layer equations and the auxiliary equations may not be expressed in inverse form.

The other approach, which may be employed using almost any inverse airfoil method, entirely dispenses with the inverse boundary-layer solution as a driver to the inverse airfoil method. In an interactive and iterative fashion, all of the design goals are achieved by carefully adjusting the velocity distribution provided as input to the inverse method. Based on feedback from successive analyses and with some experience, the velocity distribution may be changed in the direction necessary to bring the airfoil closer to the desired goals.

It is instructive to illustrate this iterative technique within the framework of the inverse airfoil design method described in Ref. 2. The method uses conformal mapping to transform the flow about the circle into that about an airfoil. A review of the theory is presented later. The circle is divided into a desired

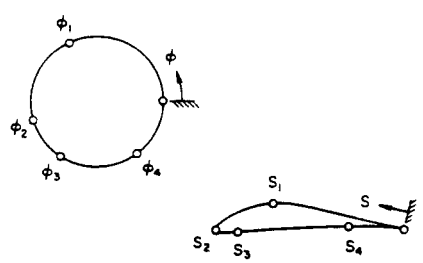

Fig. 1 Circle divided into five segments and mapped to an airfoil.

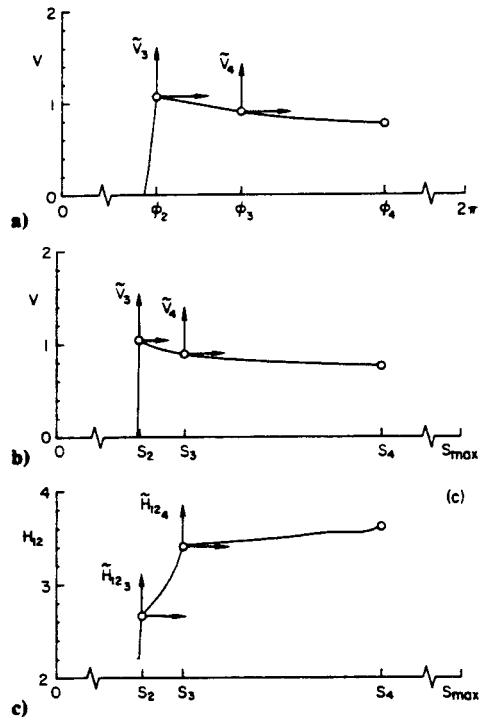

Fig. 2 Velocity distributions for the third and fourth segments at $\alpha = 5$ deg plotted as a function of a) ϕ, b) s, and c) the corresponding shape-factor distribution.

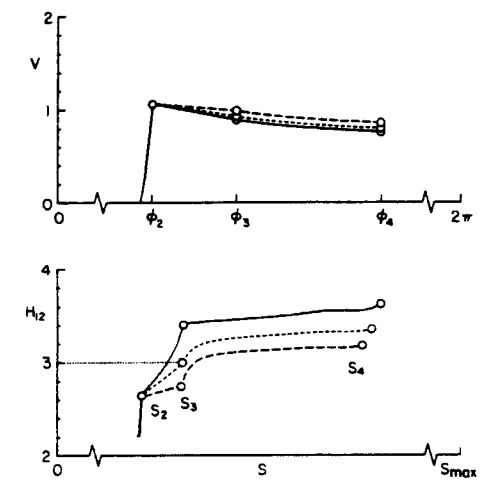

Fig. 3 Changes in the shape-factor distribution as a result of varying the slope of the velocity distribution on the third segment.

number of segments along each of which the airfoil velocity distribution as a function of the circle arc limit ϕ is prescribed for a specified angle of attack corresponding to the segment. For this example, five segments are used as depicted in Fig. 1. Attention, however, is focused only on the third and fourth segments (on the lower surface) along which the velocity is prescribed for $\alpha = 5$ deg.

The velocity distribution along any intermediate segment at the design angle of attack is made up of a constant level and a velocity distribution relative to this constant level; i.e., $v_i + \tilde{v}_i(\tilde{\phi}_i)$, where $\tilde{\phi}_i$ is the arc limit relative to the beginning of the segment i. By definition and without any loss in generality, it is taken that $\tilde{v}_i(\tilde{\phi}_i = 0) = 0$. These relative design velocity distributions are indicated in Fig. 2a for the third and fourth segments. The origin of the relative coordinate system is positioned for each segment at the constant velocity level v_i. The relative velocity is then measured from this origin. After specifying the airfoil design velocity distribution and angle of at-

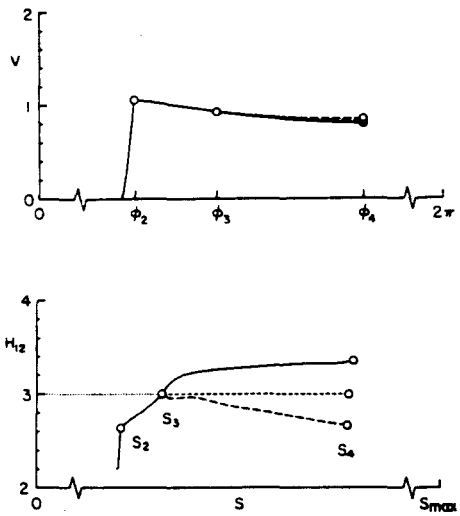

Fig. 4 Changes in the shape-factor distribution as a result of varying the velocity distribution along the fourth segment.

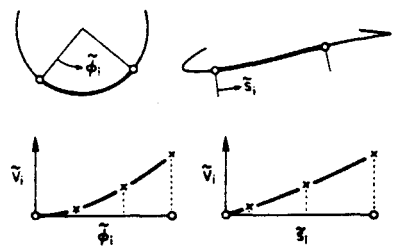

Fig. 5 Splined relative velocity distribution in terms of the circle coordinate $\tilde{\phi}_i$ and airfoil arc length $\tilde{s}_i$.

tack for each segment, the inverse problem is solved to obtain the airfoil shape. The velocity distribution may then be plotted as a function of the arc length s as shown in Fig. 2b. Figure 2c shows the resulting boundary-layer shape-factor distribution in the relative coordinate system that is consistent with the prescribed velocity distribution.

Now it is supposed that one of the design goals is to have $H_{12} = 3$ for the fourth segment at the design angle of attack $\alpha = 5$ deg. As shown in Fig. 3, the relative velocity at the end of the third segment for the airfoil of Fig. 1 may be adjusted to achieve the desired initial condition: $H_{12} = 3$. After having achieved this desired initial condition, attention is turned to adjusting to relative velocity distribution on the fourth segment so that H_{12} along the segment does not change from the initial condition. Put differently, $\tilde{v}_4(\tilde{\phi}_4)$ is adjusted to achieve $\tilde{H}_{12_4}(\tilde{s}_4) = 0$. Although it cannot be seen from Fig. 4, the solution for $\tilde{v}_4(\tilde{\phi}_4)$ which gives $\tilde{H}_{12_4}(\tilde{s}_4) = 0$ leads to a slight change in the initial condition. This process could be repeated until the shape-factor distribution for the fourth segment is within any set tolerance of the desired value of 3.

The basis of a practical inverse design method emerges from this simple example. Specifically, for the example presented, the relative velocity for the third segment is defined by one parameter—the relative velocity at the end of the segment assuming a linear variation in $\tilde{\phi}_3$. Then, the relative velocity distribution for the fourth segment is defined by a fixed number of nodes through which a spline is passed as indicated in Fig. 5. A multidimensional Newton iteration method is then used to iterate on the points defining the velocity distribution to achieve the desired initial condition $H_{12} = 3$ at the beginning of the fourth segment and $\tilde{H}_{12} = 0$ at the nodes of the fourth segment.

The approach described is precisely that taken here. This technique can be employed to achieve a desired $v(s)$,[13] but it readily generalizes to allow for the achievement of a desired boundary-layer development. Moreover, it is straightforward to include in the Newton system equations for the thickness ratio, pitching moment, or any other single parameter. The remainder of this paper reviews briefly the potential-flow inverse formulation and presents the direct boundary-layer analysis method. The multidimensional Newton iteration scheme is then discussed and one example airfoil is given.

Potential-Flow Inverse Airfoil Design Method

Eppler was the first to develop a theory for multipoint inverse airfoil design, and today the use of this method, which is based on conformal mapping, is widespread. Whereas Eppler's formulation only considers cusped trailing edges, the present theoretical development, which draws on the work of Eppler, allows for both the design of cusped and finite trailing-edge angle airfoils. Finite trailing-edge angle airfoils are permitted by including an additional factor in the conformal transformation that in turn requires the modification of the functions that control the recovery regions of the velocity distribution. The formulation of the numerical solution also differs. For the intermediate airfoil segments, that is, all segments excluding the first and last, the design velocity distribution for the segment can be a prescribed function as indicated in Figs. 2a and 5. Eppler's formulation only permits a constant design velocity for an intermediate segment at the design angle of attack. Finally, the current method employs multidimensional Newton iteration to solve the resulting system of nonlinear equations and to enable the designer to achieve a multitude of design requirements.

Theoretical Development

A summary of the inverse method, fully detailed in Ref. 13, begins by considering the complex velocity in the airfoil plane expressed as

$$\frac{dF}{dz} = \frac{dF/d\zeta}{dz/d\zeta} \tag{1}$$

On the boundary of the unit circle, $\zeta = e^{i\phi}$, this becomes

$$\left(\frac{dF}{dz}\right)_{e^{i\phi}} = \frac{(dF/d\zeta)_{e^{i\phi}}}{(dz/d\zeta)_{e^{i\phi}}} \tag{2}$$

where $0 \le \phi \le 2\pi$. From potential-flow theory, the complex velocity on the circle is expressed as

$$\left(\frac{dF}{d\zeta}\right)_{e^{i\phi}} = 4 \sin\frac{\phi}{2}\left|\cos\left[\frac{\phi}{2} - \alpha^*(\phi)\right]\right| \exp\left\{-i\left[\phi - \frac{\pi}{2} - \pi^*(\phi)\right]\right\} \tag{3}$$

where

$$\pi^*(\phi) = \begin{cases} 0, & 0 \le \phi \le \pi + 2\alpha^*(\phi) \\ \pi, & \pi + 2\alpha(\phi) \le \phi \le 2\pi \end{cases} \tag{4}$$

The quantity in the exponent, $\phi - \pi/2 - \pi^*(\phi)$, is the flow angle about circle. The step function $\pi^*(\phi)$ is included to account for the 180-deg jumps in the flow angle at the forward and rear stagnation points. For single-point design $\alpha^*(\phi)$ is a constant and may be considered as the design angle of attack in the usual manner. For practical multipoint design, however, $\alpha^*(\phi)$ is considered a piecewise function. For each segment of the airfoil there corresponds a constant, design angle of attack, α_i. The design angle-of-attack distribution $\alpha^*(\phi)$ is the function made up of these individual design angles of attack α_i about the airfoil. The desired velocity distribution on the airfoil is expressed in exponential form as

$$\left(\frac{dF}{dz}\right)_{e^{i\phi}} = v^*(\phi) \exp[-i\theta^*(\phi)] \tag{5}$$

Since the velocity distribution about the circle is known and the velocity distribution about the airfoil is specified, it re-

mains to determine the derivative of the mapping function through Eq. (2) in order to obtain the corresponding airfoil shape. The derivative of the transformation is assumed to be of the form

$$\frac{dz}{d\zeta} = \left(1 - \frac{1}{\zeta}\right)^{1-\epsilon} \exp \sum_{m=0}^{\infty} (a_m + ib_m)\zeta^{-m}, \quad |\zeta| \geq 1 \tag{6}$$

hat on the boundary of the circle becomes

$$\left(\frac{dz}{d\zeta}\right)_{e^{i\phi}} = (1 - e^{-i\phi})^{1-\epsilon} \exp[P(\phi) + iQ(\phi)] \tag{7}$$

Substitution of Eqs. (3), (5), and (7) into Eq. (2) leads to

$$P(\phi) = -\ell_n \left\{ \frac{2 \sin \phi/2^{-\epsilon} v^*(\phi)}{2|\cos[\phi/2 - \alpha^*(\phi)]|} \right\} \tag{8}$$

Consideration of airfoil closure and compatibility between e specified velocity distribution and the freestream leads to the three integral constraints given by

$$\int_0^{2\pi} P(\phi) \begin{Bmatrix} 1 \\ \cos\phi \\ \sin\phi \end{Bmatrix} d\phi = \begin{Bmatrix} 0 \\ 1-\epsilon \\ 0 \end{Bmatrix} \tag{9}$$

Consequently the airfoil velocity distribution $v(\phi)$ and angle of attack distribution $\alpha^*(\phi)$ may not be specified arbitrarily but must satisfy these three equations. In addition, as seen ough Eq. (8), the function $P(\phi)$ must be continuous in order that the velocity distribution be continuous at any single angle of attack. Having specified $P(\phi)$ through $v^*(\phi)$ and $\alpha^*(\phi)$ subject to these three integral constraints and the condition that $P(\phi)$ be continuous, the conjugate harmonic function $Q(\phi)$ is determined through application of Poisson's integral. The functions $P(\phi)$ and $Q(\phi)$ define the derivative of the mapping function which may be integrated about the circle to give the airfoil coordinates, $z(\phi) = x(\phi) + iy(\phi)$.

Numerical Formulation

he formulation of the numerical solution begins with the ification of the design velocity and angle-of-attack distributions. As mentioned, the design angle-of-attack distribution is specified in a piecewise manner by assigning a constant angle of attack to each segment of the airfoil. Likewise, $v^*(\phi)$ is prescribed as a piecewise function. Its form is selected on the basis that it must facilitate the numerical solution and permit the design of practical airfoils. For each segment other than the first or the last, the design velocity distribution is written in the form

$$v^*(\phi) = v_i + \tilde{v}_i(\tilde{\phi}_i), \qquad \phi_{i-1} \leq \phi \leq \phi_i \tag{10}$$

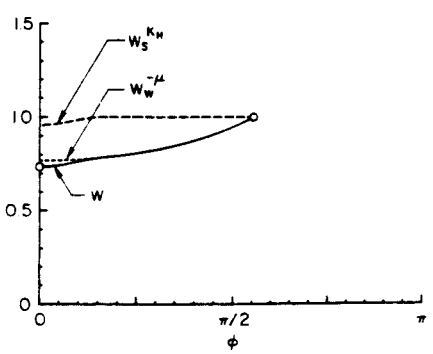

Fig. 6 Component recovery functions and total recovery function for $\phi_W = 100$, $\phi_S = 20$ deg, $\mu = 0.3$, $K_H = 0.1$, $\epsilon = 0$, and $K = 1$ corresponding to an airfoil with a cusped trailing edge.

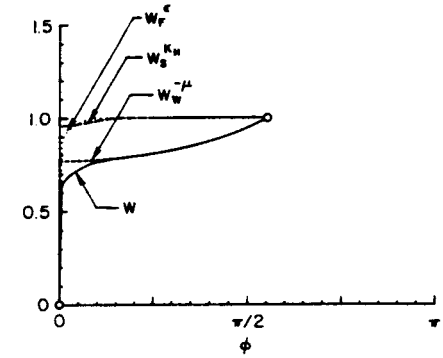

Fig. 7 Component recovery functions and total recovery function for $\phi_W = 100$, $\phi_S = 20$, $\phi_F = 10$ deg, $\mu = 0.3$, $K_H = 0.1$, $\epsilon = 1/18$, and $K = 1$ corresponding to an airfoil with a 10-deg trailing-edge angle.

as discussed in the previous example. For the first segment, the design velocity distribution is expressed as

$$v^*(\phi) = v_1 w(\phi), \qquad 0 \leq \phi \leq \phi_1 \tag{11a}$$

while for the last

$$v^*(\phi) = v_I \bar{w}(\phi), \qquad \phi_{I-1} \leq \phi \leq 2\pi \tag{11b}$$

The recovery function $w(\phi)$ for the upper surface is defined by

$$w(\phi) = w_{\bar{W}}^{\bar{\mu}}(\phi) w_S^{K_H}(\phi)\, w_F^{\epsilon}(\phi), \qquad 0 \leq \phi \leq \phi_1 \tag{12}$$

where

$$w_W(\phi) = 1 + K\left(\frac{\cos\phi - \cos\phi_W}{1 + \cos\phi_W}\right), \qquad 0 \leq \phi \leq \phi_W \tag{13a}$$

$$w_S(\phi) = \begin{cases} 1 - 0.36\left(\dfrac{\cos\phi - \cos\phi_S}{1 - \cos\phi_S}\right)^2, & 0 \leq \phi \leq \phi_S \\ 1, & \phi_S \leq \phi \leq \phi_W \end{cases} \tag{13b}$$

$$w_F(\phi) = \begin{cases} \dfrac{\sin\phi/2}{\sin\phi_F/2}, & 0 \leq \phi \leq \phi_F \\ 1, & \phi_F \leq \phi \leq \phi_W \end{cases} \tag{13c}$$

where $\phi_W \equiv \phi_1$. The recovery function $\bar{w}(\phi)$ for the lower surface is of the same form except that $w_W(\phi)$, $w_S(\phi)$, $w_F(\phi)$ and the defining parameters μ, K_H, K, ϕ_W, ϕ_S, and ϕ_F are replaced by $\bar{w}_W(\phi)$, $\bar{w}_S(\phi)$, $\bar{w}_F(\phi)$, $\bar{\mu}$, $\bar{K}_H$, $\bar{K}$, $\bar{\phi}_W \equiv \phi_{I-1}$, $\bar{\phi}_S$, and $\bar{\phi}_F$.

For a typical airfoil design, it is usually desirable to have $\phi_W > \phi_S > \phi_F$, for instance, $\phi_W = 100$, $\phi_S = 30$, and $\phi_F = 15$ deg. In this case, the first factor $w_{\bar{W}}^{\bar{\mu}}(\phi)$ in Eq. (12) controls the main part of the recovery. The second factor $w_S^{K_H}(\phi)$ controls to a great extent the velocity distribution in the vicinity of the trailing edge. If $\epsilon \neq 0$, the last factor $w_F^{\epsilon}(\phi)$ is active and results in the proper behavior of the velocity distribution up to and including the trailing-edge stagnation point. To illustrate the effect of these component functions given in Eqs. (13a-c) on the total recovery function of Eq.(12), the following values are used: $\mu = 0.3$, $K_H = 0.1$, $\epsilon = 0$, and $K = 1$. With these assigned values and those for the arc limits given previously, the total recovery function and the component functions are shown in Fig. 6. Since $\epsilon = 0$ in this case, an airfoil using this total recovery function would have a cusped trailing edge. If a 10-deg trailing-edge angle is desired, it is required that $\epsilon = 1/18$. The corresponding total recovery function and the component functions are shown in Fig. 7 where, as compared with Fig. 6, only the value ϵ has been changed.

The equations to be satisfied by an airfoil with I segments includes the three integral constraints together with I continu-

ity equations on $P(\phi)$, one coming from each junction between any two adjacent segments. Thus, in order to satisfy these $(I+3)$ equations, it is necessary to identify $(I+3)$ unknowns. Owing to the linearity of the equations, it is convenient to select μ, $\bar{\mu}$, K_H, and $\bar{K}_H$ as four of these unknowns. The remaining $(I-1)$ unknowns are selected from the I velocity levels ν_i, again owing to the linearity of the governing equations. Consequently, the inverse problem is defined completely by specifying one velocity level ν_i, all of the α_i, ϕ_i, $\bar{\nu}_i(\bar{\phi}_i)$, and the upper- and lower-surface main and closure recovery arc limits ϕ_W, $\bar{\phi}_W$, ϕ_S, and $\bar{\phi}_S$ and the recovery parameters K and $\bar{K}$. Also, if the airfoil is to have a finite trailing-edge angle, ϵ is given to yield a trailing-edge angle of $\pi\epsilon$. Also, the trailing-edge recovery arc limits, ϕ_F and $\bar{\phi}_F$, are specified to define the trailing-edge recovery function, Eq. (13c).

Throughout the remainder of this paper the specified design quantities α_i, ϕ_i, and so on, which define the potential-flow inverse design problem, are termed the inverse design parameters.

Direct Boundary-Layer Method

Once the airfoil is designed using the previously described inverse method, the boundary-layer development is then determined along each segment of the airfoil at the design condition for which some boundary-layer development is prescribed. For rapid interactive design, a direct integral boundary-layer method is used and displacement-thickness potential-flow iteration is not performed. The integral momentum and energy equations are used in the standard form:

$$\frac{d\delta_2}{ds} = -(2+H_{12})\frac{\delta_2}{\nu}\frac{d\nu}{ds} + c_f \tag{14a}$$

$$\frac{d\delta_3}{ds} = -\frac{3\delta_3}{\nu}\frac{d\nu}{ds} + c_D \tag{14b}$$

with laminar and turbulent closure relations expressed functionally as

$$H_{12} = H_{12}(H_{32}) \tag{15a}$$

$$c_f = c_f(H_{12}, Re_{\delta_2}) \tag{15b}$$

$$c_D = c_D(H_{12}, Re_{\delta_2}) \tag{15c}$$

The correlations used in the present method are taken from Ref. 22 for the laminar case and Ref. 23 for the turbulent case. The shape-factor correlation for laminar flow, however, is modified as will be discussed.

The prescribed boundary-layer developments are limited to those corresponding to attached flows. A special problem is encountered, however, if at some point in the Newton iteration laminar separation is reached before transition. An excursion of this sort is entirely conceivable even though the final boundary-layer development will be attached along the design segment at the prescribed design condition.

Conventional integral boundary-layer solution techniques switch at the point of laminar separation from a treatment of the velocity as the independent variable to its treatment as a dependent variable; that is, it follows fr. m the solution. What is given instead of the velocity is another variable, such as the shape of the separation streamline,[24] distribution of the shape factor,[25] or boundary-layer displacement thickness, all of which approximate the development of the ensuing laminar separation bubble. The integral boundary-layer equations are then solved in an inverse mode with the new variable as the independent variable. An entirely different approach is to solve the problem through the inverse boundary-layer equations by the specification of a boundary-layer variable in order to find the corresponding boundary-layer edge velocity.[8]

The need to approach the solution in either of these two ways is guided by clues found in the governing equations. The shape-factor correlation for $H_{12} = H_{12}(H_{32})$ based on the Falkner-Skan family of profiles is only valid for $H_{32} \geq 1.515$, whether or not the flow is attached or separated. An inversion of the relations given by Drela[22] yields for attached flows

$$H_{12} = -5.967105 + 6.578947\,H_{32} - \sqrt{43.2865\,(0.907 - H_{32})^2 - 16} \tag{16a}$$

for $H_{32} \geq 1.515$. For separated flows with $H_{32} > 1.515$,

$$H_{12} = -14.9375 + 12.5\,H_{32} + \sqrt{156.25\,(1.195 - H_{32})^2 - 16} \tag{16b}$$

An attempt to solve the integral boundary-layer equations beyond the point of separation with a boundary-layer edge velocity given by inviscid theory yields a shape factor $H_{32} < 1.515$, which is not within the bounds of the correlations.

To circumvent this difficulty and to integrate in the direct mode beyond the point of laminar separation, the present method replaces Eq. (16b) for separated flow with a fictitious shape-factor relation given by

$$H_{12} = 7\sqrt{1.515 - H_{32}} + 4 \tag{17}$$

for $H_{32} < 1.515$. This equation merely serves as a means to continue in the direct mode beyond laminar separation without having to resort to an inverse boundary-layer method. Of course, the solution beyond the point of laminar separation is no longer a valid boundary-layer development. Nevertheless, the final solution after iteration yields the desired (i.e., prescribed) attached boundary-layer development for which the correlations are still perfectly valid.

Transition from laminar to turbulent flow is predicted by a simplified e^n-method based on linear stability theory as discussed in Ref. 26 or the $(H-R)$ method of Eppler.[1]

Multidimensional Newton Iteration

As illustrated in the example shown in Figs. 1-4, the prescribed velocity distribution defined by the inverse design parameters ν_i, all of the α_i, ϕ_i, etc., will not necessarily result in an airfoil having all of the specified properties. With experience and painstaking manipulation of the inverse design parameters, the desired properties can be obtained provided that they are realistically achievable and compatible.

This sophisticated trial-and-error approach through the inverse method may be automated by solving the problem through multidimensional Newton iteration. Thus, control over the inverse design parameters is selectively given up; i.e., the values are determined through Newton iteration, in favor of matching desired airfoil characteristics that are not explicitly given as input to the potential-flow inverse airfoil design problem.

As illustrated in the example of Fig. 4, the shape factor H_{12} at the beginning of the fourth segment is specified as 3. This value is obtained by the adjustment of the slope $d\bar{\nu}_3/d\bar{\phi}_3$. Through Newton iteration, $d\bar{\nu}_3/d\bar{\phi}_3$ becomes the unknown in order to satisfy the Newton equation

$$d\bar{\nu}_3/d\bar{\phi}_3 \quad \Rightarrow \quad 0 = H_{12}(s_3) - 3 \tag{18}$$

where the notation "$\Rightarrow$" means that this inverse design parameter has a first-order effect on the corresponding Newton equation. It further serves as an aid in keeping an equal number of equations as unknowns.

For the fourth segment, the relative design velocity distribution $\bar{\nu}_4(\bar{\phi}_4)$ is adjusted such that $\bar{H}_{12_4}(\bar{s}_4) = 0$, that is, through Newton iteration

$$\bar{\nu}_4(\bar{\phi}_4) \quad \Rightarrow \quad 0 = \bar{H}_{12_4}(\bar{s}_4) \tag{19}$$

The numerical problem, however, must be discretized for incorporation into the Newton system. The design velocity

distribution $\tilde{v}_4(\tilde{\phi}_4)$ is defined by a desired number of moveable spline supports as shown in Fig. 5. For the three nodes shown, the following three equations must be satisfied:

$$\tilde{v}_4(\tilde{\phi}_4 = \tilde{\phi}_4^1) \quad \Rightarrow \quad 0 = \tilde{H}_{12_4}(\tilde{s}_4 = \tilde{\phi}_4^1) \tag{20a}$$

$$\tilde{v}_4(\tilde{\phi}_4 = \tilde{\phi}_4^2) \quad \Rightarrow \quad 0 = \tilde{H}_{12_4}(\tilde{s}_4 = \tilde{\phi}_4^2) \tag{20b}$$

$$\tilde{v}_4(\tilde{\phi}_4 = \tilde{\phi}_4^3) \quad \Rightarrow \quad 0 = \tilde{H}_{12_4}(\tilde{s}_4 = \tilde{\phi}_4^3) \tag{20c}$$

where the superscripts indicate the index of the nodes in terms of the arc limit $\tilde{\phi}_4$ and the corresponding nodes in $\tilde{s}_4$.

Practically any conceivable desired airfoil property can be incorporated into the Newton system with iteration on some inverse design parameter. As in the companion paper,[2] the pitching moment at a given angle of attack may be specified by the adjustment of the specified velocity level v_i as

$$\text{Only specified } v_i \quad \Rightarrow \quad 0 = c_m - p \tag{21}$$

where p is the value of the generic desired parameter, in this case the pitching moment.

An arc limit ϕ_i between two segments can be iterated to correspond to a specified x_i/c or s_i/c location as

$$\phi_i \quad \Rightarrow \quad 0 = x_i/c - p \tag{22a}$$

or

$$\phi_i \quad \Rightarrow \quad 0 = s_i/c - p \tag{22b}$$

More generally, the arc limit may be adjusted so that a specified boundary-layer property is reached at that location. For example, ϕ_i may be iterated to correspond to the point where the linear stability amplification factor n is a value of 9 for a given operating condition, i.e.,

$$\phi_i \quad \Rightarrow \quad 0 = n(s_i) - 9 \tag{23}$$

The basic inverse formulation through the specification of $v^*(\phi)$ and $\alpha^*(\phi)$ can lead to an airfoil that is crossed. Fortunately, this problem can be remedied through appropriate iteration. By empirical observation, the trailing-edge velocity ratio of uncrossed airfoils is always less than unity. Moreover, it can be shown that the thicker the airfoil, the lower the trailing-edge velocity ratio.[27] Many inverse methods make use of this fact and allow for the adjustment of an inverse design parameter in order to match a specified trailing-edge velocity ratio, which is somewhat less than unity. A shortcoming of this approach is that the airfoil thickness is not known a priori, thereby making it difficult to preassign the proper trailing-edge velocity ratio. Also specifying the trailing-edge velocity ratio is not a viable option for the design of airfoils having a finite trailing-edge angle in which case the trailing-edge velocity is always zero.

More can be deduced from the character of the trailing-edge velocity distribution than from the value of the trailing-edge velocity ratio. Figure 8 shows the trailing-edge velocity distribution and the corresponding trailing-edge shape for three, symmetric, 8% thick, cusped airfoils at a 5-deg angle of attack. Only the last 25% of chord is shown, and the vertical y/c scale has been expanded to five times that of the x/c scale. The trend is that the larger the drop in velocity (i.e., pressure recovery) at the trailing edge, the thicker the airfoil in the vicinity of the trailing edge (e.g., case *a*). If there is no drop in the velocity, the trailing edge is very thin (e.g., case *b*). If the velocity shows an increase, the airfoil is usually crossed (e.g., case *c*). Although these comments are specific to symmetric airfoils such as those shown in Fig. 8, the same trends are observed for non-symmetric airfoils as long as the net velocity drop is considered. For example, if the velocity decreases on the upper surface by the same amount that it increases on the lower surface, there is zero net velocity drop. In such an instance, the airfoil will be thin at the trailing edge.

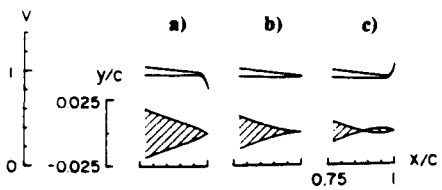

Fig. 8 Impact of the trailing-edge velocity distribution on the shape of the trailing edge: a) moderately thick trailing edge, b) thin trailing edge, and c) crossed trailing edge.

The trend just discussed must be translated into an equation if typical trailing-edge shapes are to result from the design method. The functions given in Eqs. (12) and (13) have been derived so that normal trailing-edge velocity distributions can be produced. In particular, the closure contributions, $w_S^{K_H}(\phi)$ and $\tilde{w}_S^{K_H}(\phi)$ have a dominant effect on the trailing-edge velocity distributions. By prescribing the sum $(K_H + \tilde{K}_H) = K_S$ to be in the range 0 to 0.8, normal trailing-edge velocity distributions result and give rise to uncrossed airfoils—the smaller K_S in this range, the thinner the airfoil in the vicinity of the trailing edge. Negative values for K_S usually produce crossed airfoils. To achieve the desired value of K_S, the leading-edge arc limit may be used for iteration, that is,

$$\phi_{i_{LE}} \quad \Rightarrow \quad 0 = K_S - p \tag{24}$$

For a finite trailing-edge angle ($\epsilon \neq 0$), the functions $w_F^{\epsilon}(\phi)$ and $\tilde{w}_F^{\epsilon}(\phi)$ are active and produce a zero trailing-edge velocity. It is still necessary, however, to specify K_S in order to have control over the thickness in the vicinity of the trailing edge. By these means, the designer has great control over the airfoil geometry in the region of the trailing edge.

Iteration on the design angles of attack can easily be used to control the usable lift range of the airfoil. By adding an increment to each α_i, the polar will be shifted upwards which, in turn, will decrease the zero-lift angle of attack. This shift in the polar can be controlled through a prescribed zero-lift angle of attack as

$$\alpha_i \quad \Rightarrow \quad 0 = \alpha_{OL} - p \tag{25}$$

By adding an increment to the upper surface α_i and subtracting an equal increment from the lower surface α_i, the width of the polar will be increased. This has the effect of thickening the airfoil and may be controlled through

$$\alpha_i^{\pm} \quad \Rightarrow \quad 0 = t/c - p \tag{26}$$

where $\pm$ means to adjust the α_i in opposite fashion.

The relative design velocity distribution for a segment may be used to control the relative boundary-layer shape-factor distribution as previously mentioned, or the relative velocity distribution in $\tilde{s}_i$,[2] or any one of other desired distributions. For example, either the local airfoil geometry may be specified, the n-development, or a curve in the H–R diagram used by Eppler for predicting transition. Through iteration on the preceding segment, the initial value is set as previously explained for the specification of the shape-factor distribution.

In the design of a new airfoil, the iterative process is taken in stages. In a typical case, K_S is first satisfied in order for the airfoil to be uncrossed. Then c_m is sometimes specified to bring the airfoil into a normal range. After this, any desired initial segment conditions are added to the Newton system before iterating on the segments that have a specified distribution of some type. If only a few small changes are made to the inverse design parameters of a converged solution, it usually is possible to iterate on the full Newton system from the outset. The convergence of the solution can be disrupted if the Newton scheme attempts to take a step that is too large. To prevent

this from happening, a maximum step size for any of the unknowns can be preset. If any of the predicted step sizes at any point in the iteration exceeds a preset maximum, then a fractional step is taken to avoid exceeding a maximum. Because the method incorporates an incompressible inverse airfoil design method and an integral boundary-layer method, the convergence is quite rapid and easily allows for the interactive design of a wide range of specialized airfoils.

Demonstration of the Method

To illustrate some of the capabilities of the method an example airfoil is considered. It should be stated that this airfoil only serves to illustrate the method and is not intended for practical use. The main design goals, although defined in mathematical detail later, may be stated as follows. Along the forward part of the upper surface of the airfoil, the n-development is prescribed at the design angle of attack and Reynolds number. By prescribing the linear stability amplification factor n, the extent of laminar flow and the location of transition is controlled. This is advantageous when there is interest in designing for low drag. Following this segment, a linear ramp is introduced for a different angle of attack. On the lower surface, at yet a different angle of attack, the boundary-layer shape-factor distribution is prescribed much like the example of Figs. 1-4. Specification of the boundary-layer shape factor is desirable in instances where flow separation is to be avoided.

These characteristics described are obtained using seven segments on the airfoil—four segments on the airfoil upper surface and three on the lower. All of the inverse design parameters are listed in Table 1, with the exception of the trailing-edge angle parameter ϵ. Many of the inverse design parameters listed in Table 1 are selected as unknowns in the Newton iteration in order to match the design goals, but for those that are fixed the following values are used:

$$\alpha_1 = \alpha_2 = 10 \text{ deg} \tag{27a}$$

$$\alpha_3 = \alpha_4 = 15 \text{ deg} \tag{27b}$$

$$\alpha_5 = \alpha_6 = \alpha_7 = 8 \text{ deg} \tag{27c}$$

$$K = \bar{K} = 1 \tag{27d}$$

$$\phi_S = 15 \text{ deg}, \qquad \bar{\phi}_S = 340 \text{ deg} \tag{27e}$$

$$\phi_F = 10 \text{ deg}, \qquad \bar{\phi}_F = 350 \text{ deg} \tag{27f}$$

$$\epsilon = 1/18 \tag{27g}$$

The value for ϵ is selected to yield a 10-deg trailing-edge angle and the arc limits ϕ_S, $\bar{\phi}_S$, ϕ_F, and $\bar{\phi}_F$ are set to confine the closure and the finite trailing-edge angle contributions of the pressure recovery to a small region near the trailing edge. The small values for K and $\bar{K}$, which partly define the main pressure recovery, will give a slight adverse pressure gradient at the beginning of the recovery on the upper and lower surfaces at the corresponding design angles of attack, α_1 and α_7, respectively.

As discussed in the preceding section, the design goals are matched in stages. In this example case, the process is taken in the order of increasing complexity. First, the leading-edge arc limit is iterated to match K_S. Afterwards, the leading-edge arc limit ϕ_4 and the specified velocity level v_i are iterated together to achieve the design K_S and c_{m_0} as

$$\phi_4 \quad \Rightarrow \quad 0 = K_S - 0.4 \tag{28a}$$

$$\text{Only specified } v_i \quad \Rightarrow \quad 0 = c_{m_0} + 0.25 \tag{28b}$$

Next, the remaining arc limits are iterated to correspond to specified s_i/c locations by

$$\phi_1 \quad \Rightarrow \quad 0 = s_1/c - 0.25 \tag{29a}$$

$$\phi_2 \quad \Rightarrow \quad 0 = s_2/c - 0.40 \tag{29b}$$

$$\phi_3 \quad \Rightarrow \quad 0 = s_3/c - 0.90 \tag{29c}$$

$$\phi_5 \quad \Rightarrow \quad 0 = s_5/c - 1.20 \tag{29d}$$

$$\phi_6 \quad \Rightarrow \quad 0 = s_6/c - 1.70 \tag{29e}$$

After this, the relative design velocity distribution on the second segment is included for iteration to produce a linear velocity distribution in s at the design angle of attack $\alpha_2 = 10$ deg. Specifically,

$$\bar{v}_2(\bar{\phi}_2) \quad \Rightarrow \quad 0 = \bar{v}_2(\bar{s}_2) + 1.2\bar{s}_2 \tag{30}$$

where now $\bar{s}_2$ is measured in the direction from s_2 to s_1, that is, $\bar{s}_2 = s_2 - s$ (opposite to that shown in Fig. 5). Figure 9 shows portions of the velocity distribution extending from the stagnation point for the design angles of attack $\alpha = 8$, 10, and 15 deg. For the 10-deg case, it is seen in the figure that the desired linear variation (in boldline) is obtained for the second segment. The $\alpha = 8$ and 15-deg cases are pertinent to the remaining lower-surface and upper-surface design requirements, respectively.

For the lower surface, the boundary-layer shape factor is prescribed to be $H_{12} = 2.8$ for the sixth segment at $\alpha_6 = 8$ deg. This is achieved, as in the illustrated example of Figs. 1-4, by iterating on the preceding segment to match the desired initial condition and by adjusting the relative velocity distribution along the sixth segment to maintain $H_{12} = 2.3$, that is,

$$d\bar{v}_5/d\bar{\phi}_5 \quad \Rightarrow \quad 0 = H_{12}(s_5) - 2.8 \tag{31a}$$

$$\bar{v}_6(\bar{\phi}_6) \quad \Rightarrow \quad \bar{0} = \bar{H}_{12_6}(\bar{s}_6) \tag{31b}$$

As shown in Fig. 10, this shape-factor distribution is achieved by the velocity distribution shown in Fig. 9 for $\alpha = 8$ deg.

On the upper surface, the n-development is prescribed for the third segment at the design conditions $\alpha_3 = 15$ deg and

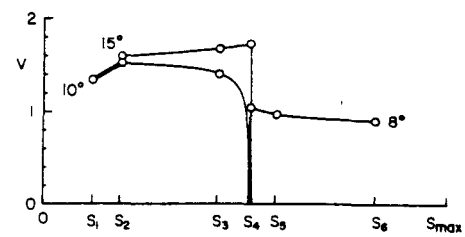

Fig. 9 Partial velocity distributions corresponding to the design conditions ($s_{max} = 2.067$).

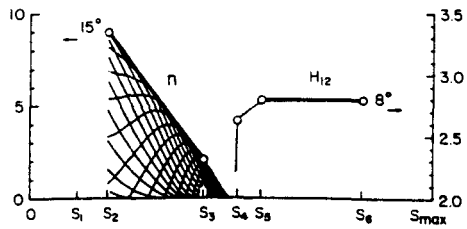

Fig. 10 Partial boundary-layer developments corresponding to the design conditions ($R = 1 \times 10^6$ for the n-development).

Table 1 Inverse design parameters for a seven-segment airfoil

i	ϕ	$\alpha^*(\phi)$	$v^*(\phi)$
1	$[0, \phi_1]$	α_1	v_1, $w(\phi; \phi_W, \phi_S, \phi_F, \mu, K_H, K)$
2	$[\phi_1, \phi_2]$	α_2	v_2, $\bar{v}_2(\bar{\phi}_2)$
3	$[\phi_2, \phi_3]$	α_3	v_3, $\bar{v}_3(\bar{\phi}_3)$
4	$[\phi_3, \phi_4]$	α_4	v_4, $\bar{v}_4(\bar{\phi}_4)$
5	$[\phi_4, \phi_5]$	α_5	v_5, $\bar{v}_5(\bar{\phi}_5)$
6	$[\phi_5, \phi_6]$	α_6	v_6, $\bar{v}_6(\bar{\phi}_6)$
7	$[\phi_6, 2\pi]$	α_7	v_7, $\bar{w}(\phi; \bar{\phi}_W, \bar{\phi}_S, \bar{\phi}_F, \bar{\mu}, \bar{K}_H, \bar{K})$

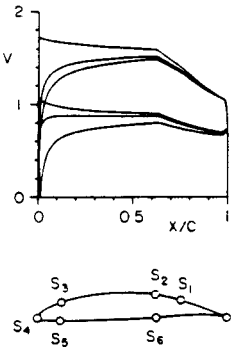

Fig. 11 Airfoil and velocity distributions for $\alpha = 8$, 10, and 15 deg.

$R_1 = 1 \times 10^6$. The initial value of $n = 2$ is set by adjusting the velocity distribution of the fourth segment, i.e.,

$$d\tilde{v}_4/d\tilde{\phi}_4 \quad \Rightarrow \quad 0 = n(s_3) - 2 \tag{32}$$

The velocity distribution for the third segment is adjusted to give the desired linearly increasing n-growth given by

$$\tilde{v}_3(\tilde{\phi}_3) \quad \Rightarrow \quad 0 = \tilde{n}_3(\tilde{s}_3) - 14\tilde{s}_3 \tag{33}$$

where $\tilde{s}_3$ is measured from s_3 to s_2, that is, $\tilde{s}_3 = s_3 - s$.

Since the length of the segment is $s_3 - s_2 = 0.5$ and the initial value is $n = 2$, this gives $n = 9$ at the end of the segment to correspond to the point of transition. As shown in Fig. 10, this desired n-growth, based on the analysis method of Ref. 26, is achieved. Finally, the airfoil shape and the velocity distributions at the design angles of attack are shown in Fig. 11.

Conclusions

A hybrid-inverse airfoil design technique has been developed by coupling a potential-flow, multipoint inverse airfoil design method with a direct boundary-layer analysis method. The potential-flow inverse design parameters can be iteratively adjusted automatically through multidimensional Newton iteration in order to obtain desired airfoil characteristics that are not explicitly given as input to the potential-flow inverse method. This combined approach makes it possible to prescribe along segments of the airfoil either the local geometry or, together with the design conditions, the velocity distribution or some boundary-layer development. At the same time it is possible to specify single parameters such as thickness ratio or pitching moment. Although the current implementation of this approach makes use of an incompressible inverse design method and a direct integral boundary-layer method together with an e^n-method for transition prediction, either component could be replaced by an alternative design or analysis method. For instance, the method could be extended to handle compressible airfoil design, multielement airfoil design, or allow for the design of airfoils with regions of separated flow. As it stands, fairly sophisticated airfoil design studies can now be made with relative ease. This should ultimately lead to improvements in new airfoil designs.

Acknowledgment

The support of the NASA Langley Research Center under Grant NGT-50341 is gratefully acknowledged.

References

[1]Eppler, R., *Airfoil Design and Data*, Springer-Verlag, Berlin, Heidelberg, Germany, 1990, Chap. 3.

[2]Selig, M. S., and Maughmer, M. D., "A Multi-Point Inverse Airfoil Design Method Based on Conformal Mapping," *AIAA Journal*, Vol. 30, No. 5, 1992, pp. 1162–1170; also AIAA Paper 91-0069.

[3]Drela, M., "Viscous and Inviscid Inverse Schemes Using Newton's Method," *AGARD-FPD-VKI Lecture Series on Inverse Methods in Airfoil Design for Aeronautical and Turbomachinery Applications*, von Kármán Institute for Fluid Dynamics, Rhode-Saint-Genèse, Belgium, May 1990.

[4]Ghielmi, L., Marazzi, R., and Baron, A., "A Tool for Automatic Design of Airfoils in Different Operating Conditions," AGARD CP-463, March 1990.

[5]Wortmann, F. X., "Progress in the Design of Low Drag Airfoils," *Boundary Layer and Flow Control*, edited by G. V. Lachmann, Pergamon, London, 1961, pp. 748–770.

[6]Henderson, M. L., "Inverse Boundary-Layer Technique for Airfoil Design," NASA CP-2045, Pt. 1, Vol. 1, March 1978, pp. 383–397.

[7]Goettsching, L., "Designs of Profiles for Cascades," NASA TT-20161, April 1988.

[8]Stock, H. W., "An Inverse Boundary-Layer Method for Turbulent Flows on Infinite Swept Wings," *Z. Flugwiss.*, Vol. 12, 1988, pp. 51–62.

[9]Selig, M. S., Maughmer, M. D., and Somers, D. M., "An Airfoil for General Aviation Applications," *Proceedings of the 1990 AIAA/FAA Joint Symposium on General Aviation Systems* (Ocean City, NJ), DOT/FAA/CT-90/11, May 1990, pp. 280–291.

[10]Somers, D. M., "Subsonic Natural-Laminar-Flow Airfoils," *Natural Laminar Flow and Laminar Flow Control*, edited by R. W. Barnwell and M. Y. Hussaini, Springer-Verlag, New York, 1992.

[11]Liebeck, R. H., "On the Design of Subsonic Airfoils for High Lift," AIAA 9th Fluid and Plasma Dynamics Conference (San Diego, CA), AIAA Paper 76-406, July 1976.

[12]Drela, M., "Elements of Airfoil Design Methodology," *Applied Computational Aerodynamics*, edited by P. A. Henne, Vol. 125, Progress in Astronautics and Aeronautics, AIAA, Washington, DC, 1990, pp. 167–189.

[13]Selig, M. S., "Multi-Point Inverse Design of Isolated Airfoils and Airfoils in Cascade in Incompressible Flow," Ph.D. Thesis, Dept. of Aerospace Engineering, Pennsylvania State Univ., University Park, PA, May 1992.

[14]Mangler, W., "Die Berechnung eines Tragfügelprofiles mit vorgeschreibener Druckverteilung," *Jahrbuch der deutschen Luftfahrtforschung*, Vol. 1, 1938, pp 46–53; also Air Ministry of London, Translation No. 932, 1940.

[15]Lighthill, M. J., "A New Method of Two-Dimensional Aerodynamic Design," Aeronautical Research Council, Great Britain, R&M 2112, April 1945.

[16]Timman, R., "The Direct and Inverse Problem of Airfoil Theory. A Method to Obtain Numerical Solutions," Rept. F. 16, National Aeronautical Research Inst., The Netherlands, 1951.

[17]Eppler, R., "Direct Calculation of Airfoils from Pressure Distribution," NASA TT F-15, 417, 1974. (Translated from *Ingenieur-Archive*, Vol. 25, No. 1, 1957, pp. 32–57.)

[18]Nonweiler, T. R. F., "A New Series of Low-Drag Aerofoils," Aeronautical Research Council, Great Britain, R&M 3618, March 1968.

[19]Ingen, J. L. van, "A Program for Airfoil Section Design Utilizing Computer Graphics," *AGARD-VKI Short Course on High Reynolds Number Subsonic Aerodynamics*, AGARD LS-37-70, von Kármán Inst. for Fluid Dynamics, Rhode-Saint-Genèse, Belgium, April 1969.

[20]Arlinger, G., "An Exact Method of Two-Dimensional Airfoil Design," SAAB, Sweden, TN 67, Oct. 1970.

[21]Strand, T., "Exact Method of Designing Airfoil with Given Velocity Distribution in Incompressible Flow," *Journal of Aircraft*, Vol. 10, No. 11, 1973, pp. 651–659.

[22]Drela, M., and Giles, M. B., "Viscous-Inviscid Analysis of Transonic and Low Reynolds Number Airfoils," *Journal of Aircraft*, Vol. 25, No. 10, 1987, pp. 1347–1355.

[23]Eppler, R., and Somers, D. M., "A Computer Program for the Design and Analysis of Low-Speed Airfoils," NASA TM-80210, Aug. 1980.

[24]Ingen, J. L. van, "On The Calculation of Laminar Separation Bubbles in Two-Dimensional Incompressible Flow," AGARD CP-168, Nov. 1975.

[25]Dini, P., "A Computationally Efficient Modeling of Laminar Separation Bubbles," Ph.D. Thesis, Dept. of Aerospace Engineering, Pennsylvania State Univ., University Park, PA, 1990.

[26]Dini, P., Selig, M. S., and Maughmer, M. D., "Simplified Linear Stability Transition Prediction Method for Separated Boundary Layers," *AIAA Journal*, Vol. 30, No. 8, 1992, pp. 1953–1961.

[27]Maughmer, M. D., "Trailing Edge Flow Conditions as a Factor in Airfoil Design," Ph.D. Thesis, Dept. of Aeronautical and Astronautical Engineering, Univ. of Illinois at Urbana-Champaign, IL, May 1984.